Research Article

Nano Research
2020, 13(2): 412–418

ISSN 1998-0124 CN 11-5974/O4
https://doi.org/10.1007/s12274-020-2623-1

Revealing the anion intercalation behavior and surface evolution of graphite in dual-ion batteries via *in situ* AFM

Kai Yang[1,§], Langlang Jia[1,§], Xinhua Liu[2], Zijian Wang[1], Yan Wang[1], Yiwei Li[1], Haibiao Chen[1], Billy Wu[2], Luyi Yang[1] (✉), and Feng Pan[1] (✉)

[1] *School of Advanced Materials, Peking University Shenzhen Graduate School, Shenzhen 518055, China*
[2] *Dyson School of Design Engineering, Imperial College London, London SW7 2AZ, UK*
[§] *Kai Yang and Langlang Jia contributed equally to this work.*

Received: 14 October 2019 / **Revised:** 19 December 2019 / **Accepted:** 22 December 2019

ABSTRACT

Graphite as a positive electrode material of dual ion batteries (DIBs) has attracted tremendous attentions for its advantages including low lost, high working voltage and high energy density. However, very few literatures regarding to the real-time observation of anion intercalation behavior and surface evolution of graphite in DIBs have been reported. Herein, we use *in situ* atomic force microscope (AFM) to directly observe the intercalation/de-intercalation processes of PF_6^- in graphite in real time. First, by measuring the change in the distance between graphene layers during intercalation, we found that PF_6^- intercalates in one of every three graphite layers and the intercalation speed is measured to be 2 $\mu m \cdot min^{-1}$. Second, graphite will wrinkle and suffer structural damages at high voltages, along with severe electrolyte decomposition on the surface. These findings provide useful information for further optimizing the capacity and the stability of graphite anode in DIBs.

KEYWORDS

dual ion battery, *in situ* atomic force microscope (AFM), graphite positive electrode, hierarchical anion intercalation, structure evolution, surface reaction

1 Introduction

To meet the increasing demand of high-performance energy storage, especially for electric vehicles, novel electrode materials that of high performance and abundant resource are in great need. Dual ion batteries (DIBs) have drawn great interests of researchers due to their low costs and high energy densities [1]. Different from traditional lithium-ion batteries (LIBs) [2] the reactions at the positive electrode of DIBs involve reversible anion (e.g., PF_6^- [3], ClO_4^- [4, 5], FSI^- [6], $TFSI^-$ [7], AlF_4^- [8] and $Al_xCl_y^-$ [9–12]) intercalation/de-intercalation in layered materials (e.g., graphite).The intercalation/de-intercalation behavior of the anions in DIBs generally enable a high average potential, which lead to improved high energy densities.

Many advanced characterization tools have been used to study the reaction and intercalation mechanism in graphite-based non-aqueous DIBs. Winter [13, 14] and co-workers employed *in situ* X-ray diffraction (XRD) to study structure and compositional changes upon different anions insertion and de-insertion processes in graphite. Wang [5] et al. utilized *in situ* Raman to detect the structural change of graphite after ClO_4^- intercalation in different solvents (propylene carbonate (PC), *γ*-butyrrolactone (GBL) and ethylene carbonate (EC)), and they found that EC suppresses the anion intercalation. Wang [15] et al. utilized *in situ* electrochemical quartz crystal microbalance (EQCM) to probe the intercalation scenario of EC and PC solvated BF_4^- into graphite. Other than structural and electrochemical information, changes in surface morphology are also important for revealing the reaction mechanisms of electrodes in DIBs. Fang [16] et al. observed the thickness evolution of graphite-based positive electrode in DIBs by using real-time optical microscope and electrode volume expansion was observed after cycling. However, it is challenging for optical microscope to resolve details at the nanoscale. Although many reliable analytical results have been reported in DIBs study, they lack direct and *in situ* observation to monitor the anion intercalation and surface evolution during the entire process. In recent years, *in situ* atomic force microscope (AFM) has been considered a powerful characterization tool to visualize the evolution of the electrode surface and electrolyte decomposition during electrochemical processes in LIBs [17–21]. *In situ* AFM has great advantages in simulating the process in a real device at the nanoscale. *In situ* AFM have been used to investigate the anion intercalation in HOPG in aqueous solutions before [22–24]. ClO_4^- and HSO_4^- anions could intercalate in to the highly oriented pyrolytic graphite (HOPG) and cause graphite structure evolution. Inspired by their works, *in situ* AFM can be utilized to study the intercalation mechanism in non-aqueous DIBs.

In this work, *in situ* AFM is employed to investigate the PF_6^- anion intercalation/de-intercalation processes in HOPG in carbonate electrolyte. By measuring the changes in the thickness of HOPG layers at different voltages, the hierarchy anion intercalation behavior as well as the speed of PF_6^- anion intercalation within the graphite layers can be characterized. In addition, decomposition of the electrolyte and graphite

Address correspondence to Luyi Yang, yangly@pkusz.edu.cn; Feng Pan, panfeng@pkusz.edu.cn

distortions are directly observed.

Table S6 in the Electronic Supplementary Material (ESM) summarizes the characterization techniques previously utilized in DIBs research. Compared with techniques such as XRD and Raman, which are utilized to reveal the intercalation mechanism based on bulk size particle, our work provides direct proof of the intercalation behavior of anions in graphite electrode of DIBs at the nanoscale. These findings will be potentially useful for optimizing the capacity and the stability of graphite electrode in DIBs and similar energy storage devices.

2 Experimental

The setup of the *in situ* AFM cell is shown in Fig. 1. The highly oriented pyrolytic graphite (HOPG, 12 mm × 12 mm, ZYB Grade, Bruker Corporation) was situated at the bottom of the AFM fluid cell (MMTMEC, Bruker Corporation) as the working electrode as shown in Fig. 1(b). Natural graphite was too rough to be used as a substrate for AFM. As a special type of graphite, HOPG has a smooth and chemically homogeneous surface which is a graphite basal plane with edge sites. Therefore, it is an ideal substrate for AFM analysis which serves as a compromise between satisfying imaging capabilities and closely simulating the real graphite surfaces. The HOPG substrate was cleaved with adhesive tape to expose a fresh surface before electrochemical tests. The lithium ring encircled in the cell was used as the reference and the counter electrode. 0.1 mL of electrolyte (1 M $LiPF_6$ in EC/dimethyl carbonate (DMC), volume ratio of 1:1) was injected into the cell in each test. The electrodes were connected to a CHI1030C electrochemical workstation (Chenhua Instument Co., Ltd., China) for cyclic voltammetry (CV) tests. AFM images were taken by using a Bruker Multimode 8 system with a Nanoscope V controller and a silicon nitride modified scanning probe (f_0 = 150 kHz, k = 0.7 N·m^{-1}). The *in-situ* AFM experiments were carried out in an argon filled glovebox (MIKOUNA, H_2O < 0.1 ppm, O_2 < 0.1 ppm) at room temperature. AFM was operated in Scanasyst-fluid mode at a specific scan rate in specific voltage ranges. The images were captured at a scan rate of 0.5 Hz. AFM topography was collected in Scanasyst-fluid mode simultaneously, where direct force control at ultra-low forces helps protect delicate samples and tips from damage. The AFM probe was coated with silicon nitride, and will not affect the electrochemical process. After the *in situ* AFM tests, the HOPG was removed from the cell and washed with DMC to remove the residual electrolyte on the surface.

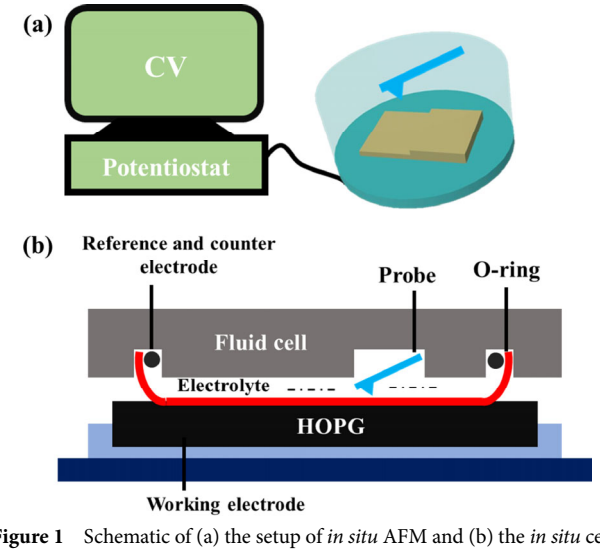

Figure 1 Schematic of (a) the setup of *in situ* AFM and (b) the *in situ* cell.

The resulting HOPG was dried in an argon filled glovebox before characterization. The X-ray photoelectron spectra (XPS) of the decomposition product was acquired on a Thermo Fisher ESCALAB 250X analysis system.

The real cell performance was analyzed by coin cells using graphite (Aladdin) as the positive electrode. A portion of N-methly-2-pyrrolidone (NMP) was added to a mixture of 90 wt.% graphite, 8 wt.% conductive carbon black and 2 wt.% pdyvinylidene fluoride (PVDF) as binder to form a homogeneous slurry. Then the slurry was coated on Al foil (Shenzhen Kejing), followed by drying at 80 °C for 24 h under vacuum. Lithium foil was used as the counter electrode and a glass fiber was used as the separator. 120 μL of electrolyte (1 M $LiPF_6$ in EC/DMC, volume ratio of 1:1) was added during cell assembling. The CV was measured at a scan rate of 2 mV·s^{-1} using a CHI1030C electrochemical workstation. The galvanostatic charge and discharge tests were conducted using a Neware battery testing system.

3 Results and discussion

3.1 *In situ* observation of reversible PF_6^- intercalation/de-intercalation in HOPG

The setup of the *in situ* AFM experiment is shown in Fig. 1. HOPG is employed as the working positive electrode, and a lithium ring serves as the counter and reference electrode. Figure 2(a) shows the image of the HOPG electrode surface scanned at the open circuit potential (OCP). Steps of different heights can be observed and each step represents a stack of graphene layers. Through height measurement and calculation, the number of graphene layers in each step can be obtained. Here, a parameter N_G is introduced to describe the number of the graphene layers in one step

$$N_G = H_0/H_{\text{single layer}} \quad (1)$$

Where H_0 is the step height measured by AFM, and it is the distance between the bottom layer and the top layer of the step. $H_{\text{single layer}}$ is the height of one single layer of graphene. More detailed definitions are listed in Table S1 in the ESM. Figure 2(b) shows the details of the measurement where Step c shows a height of 0.35 nm which can be considered as the thickness of a single layer in graphite ($H_{\text{single layer}}$ = 0.35) [25]. Therefore, for instance, since Step a is measured to be 0.7 nm, N_G in this step is calculated to be 2. Measured heights and calculated number of layers in different steps are shown in Table S2 in the ESM.

Figures 2(c)–2(e) exhibit the real-time evolution of the HOPG surface during the electrochemical process and the corresponding CV curve is presented in Fig. 2(f). Since Step c represents a single layer of graphite, it is chosen for investigating the anion intercalation/de-intercalation behaviors. As shown in Fig. 2(g), the change in height of Step c during the electrochemical process is plotted vs. voltage. The height remained constant before 4.8 V vs. Li/Li$^+$, which is the on-set potential of the anodic peak in the CV curves of both *in situ* cell (shown in Fig. 2(f)) and the *ex situ* battery (shown in Fig. S1 in the ESM). The height then increased with potential and stabilized at 0.85 nm as the voltage reached 5.5 V vs. Li/Li$^+$. The increased height of 0.5 nm is consistent with the average diameter of PF_6^- (0.45 nm) [26, 27], indicating that the height change was very likely caused by the PF_6^- anion intercalation. In the following discharge process, the height of Step c decreased to 0.35 nm as the cell was discharged back to 3.5 V vs. Li/Li$^+$, which suggests

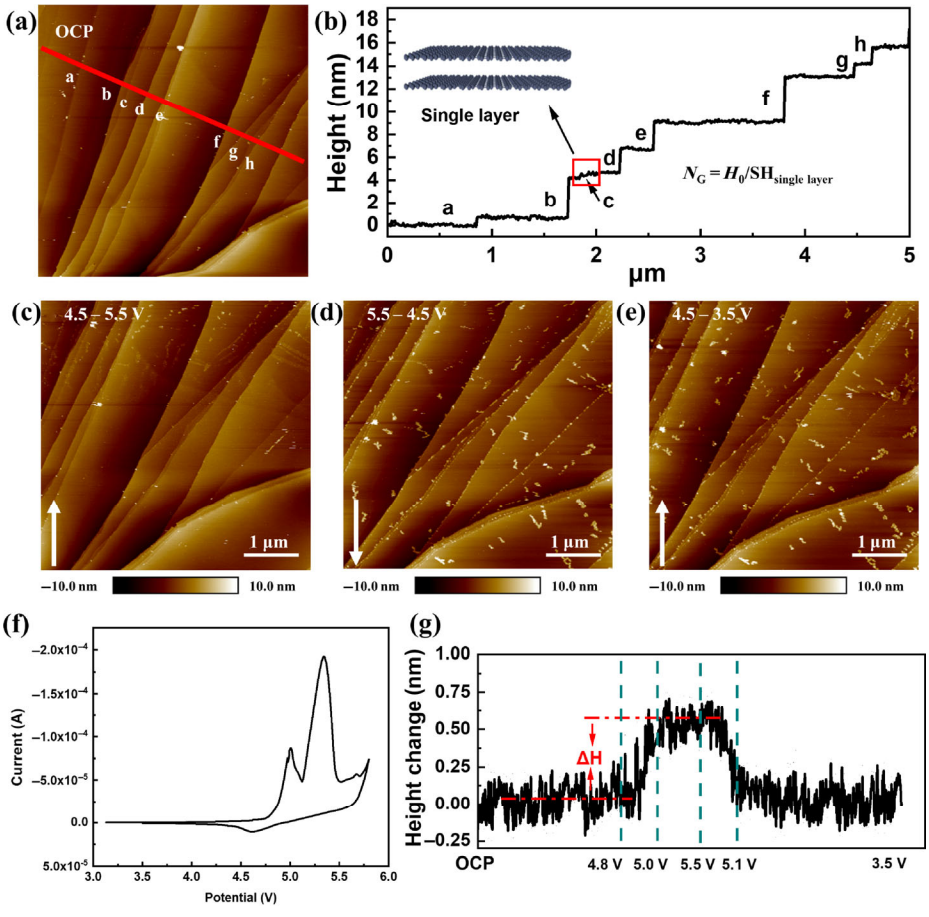

Figure 2 (a) *In situ* AFM images taken at OCP. (b) Height profile of steps labelled in (a). *In situ* AFM images taken at (c) 4.5–5.5 V, (d) 5.5–4.5 V and (e) 4.5–3.5 V, the voltage scan rate is 2 mV·s^{-1}. The white arrows show the AFM scanning direction. (f) CV curve of the *in situ* AFM test. (g) The height profile of the selected region with changing potential.

a reversible intercalation/deintercalation process in the HOPG. To exclude the physical adsorption of the anion, control experiments with no $LiPF_6$ but the same electrolyte solvent was carried out (Fig. S2 in the ESM). The height change of Step 1 is summarized in Fig. S2(d) in the ESM, and the height remained nearly unchanged during the whole CV scanning, which excludes the physical adsorption of the anion.

To further confirm the intercalation of PF_6^-, the HOPG charged to 5.5 V vs. Li/Li$^+$ was taken out for XPS measurement. In Fig. S3 in the ESM, the surface of HOPG shows no obvious signal of PF_6^-. As shown in Fig. S3 in the ESM, after being etched for 10 s, a peak at 688 eV [28] arises, which can be assigned to the existence of PF_6^-. Hence, the XPS results confirmed the intercalation of PF_6^-.

Since the anion intercalation happened at 4.8 V, we carried out *in situ* AFM test at a fixed potential of 4.8 V to observe the time dependent intercalation process. The results are shown in Figs. S4 and S5 in the ESM, where each AFM image (5 μm × 5 μm) takes 10 min to record and the white arrows in the AFM images indicate the scan direction. During the continuous AFM scanning, the height evolution is recorded. As shown in Fig. S4(a) in the ESM, the HOPG surface is flat and no anion intercalation takes place at OCP. The height evolution along the selected step (dashed line in Fig. S4(c) in the ESM) is shown in Fig. S4(d) in the ESM and the height increase is found to occur at 5 min. Figure S5 in the ESM records the following height evolution. It can be seen that at 6 min, the anion intercalation created a length of 0.2 μm, whereas at 8 min, the intercalated length is 0.6 μm, so the intercalation speed is calculated to be 0.2 μm·min^{-1} approximately.

3.2 Statistical investigation of PF_6^- intercalation behavior

With the information of single-layer intercalation obtained above, what can we learn about the multi-layer intercalation behavior? As shown in Fig. 3(c), several parameters to describe the intercalated structure are defined

$$\Delta H = H_{final} - H_0 \quad (2)$$

Where ΔH is the height change during the electrochemical process, H_0 is the original height of the graphite steps and H_{final} is the final height. Based on the previous results, the height change in a single layer caused by PF_6^- intercalation (ΔH_{anion}) can be regarded as a constant (ΔH_{anion} = 0.5 nm).

Figure S6(a) in the ESM shows that the height of Step A increased to 12.6 nm (H_{final}) compared to its original height of 8.4 nm (i.e., N_G = 24) when charged to 5.5 V vs. Li/Li$^+$. Under the assumption that the thickness change is solely contributed by the anion intercalation, the number of layers (N_I) inserted by anions can be expressed by

$$N_I = \Delta H/\Delta H_{anion} \quad (3)$$

In this case, N_I for Step A was calculated to be 8 (Fig. S6(b) in the ESM). In this case, one third of the graphite layers in Step A were intercalated with anions. A question can be then raised: is this a general pattern or merely a coincidence? In order to obtain statistically significant correlation between N_G and N_I, additional experiments and measurements for other steps were carried out and the results are shown in Fig. S7 in the ESM and summarized in Table S3 in the ESM.

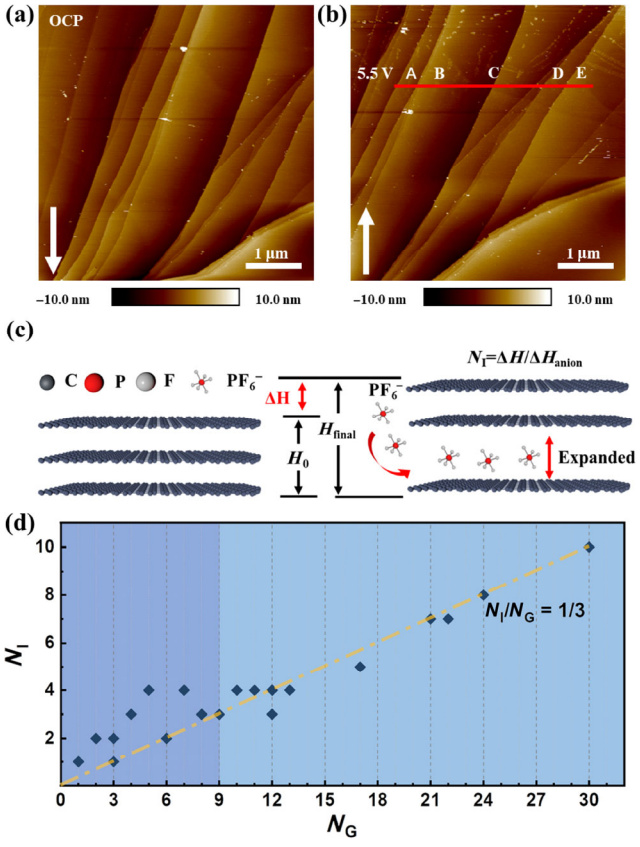

Figure 3 Anion intercalation measurement. AFM images taken at OCP (a) and 5.5 V (b), five spots (A–E) are labelled out for calculation. (c) Descriptions of several parameters related to intercalation process. (d) Statistic summarizations of NG, corresponding NI at cut-off potential of 5.5 V with several *in situ* AFM tests.

In order to conduct a reliable quantitative analysis, additional parallel *in situ* AFM tests were carried out and summarized in Table S4 in the ESM. The relationship between N_G and N_I is plotted in Fig. 3(d), where it is found that at a relatively low N_G (< 9), the N_I/N_G ratio (S_N) appears to be randomly distributed; whereas at a higher N_G (> 9), the value of S_N is very close to 1/3, suggesting that PF_6^- anion intercalates in one of every three graphene layers. The deviation at a low N_G could be attributed to the lack of sample capacity, which leads to low statistical significance and measuring errors.

Table S5 in the ESM summarized the different anion intercalation results in graphite in literatures. D. Alliata [22, 23] et al. employed the *in situ* AFM to investigate the ClO_4^- and HSO_4^- intercalation in graphite in aqueous electrolyte. They found the stage-IV GIC formation of ClO_4^- and HSO_4^- in HOPG. In many other works, the graphite interlayer spacing was measured and calculated by XRD. Different anion size and structure would affect the final GIC stage in graphite. In our work, the intercalation of PF_6^- will increase the interlayer between two graphenes by 0.5 nm which is consistent with previous works [27]. Moreover, we carried out a fixed potential scaning to measure the PF_6^- anion intercalation speed (0.2 μm·min^{-1}) within the graphene layers.

The similar hierarchical intercalation behavior of PF_6^- in graphite in non-aqueous DIBs were previously observed by means of Raman measurements [5] and dynamic functional theory (DFT) simulations [6]. However, they were not able to reveal the intercalation/deintercalation mechanism at the nanoscale. In this work, we utilized *in situ* AFM to directly observe the intercalation process and obtained quantitative results in non-aqueous electrolyte. While most of *in situ* AFM studies in lithium battery filed focus on the interfacial morphology, we demonstrated that the *in situ* AFM can be useful in analyzing the intercalation process and potentially can be employed to investigate other layered energy storage materials besides graphite.

3.3 Stability of electrolyte and graphite positive electrode

Generally, anion intercalation in graphite positive electrode occurs at a relatively high potential (> 4.5 V vs. Li/Li$^+$) [4], at which the electrolyte is prone to decomposition. As shown in Fig. 2, nano-sized residues formed along the steps of the HOPG and then on the HOPG surface and gradually grew as the potential increased during the first charging process. These residues cannot be removed by negatively sweeping the voltage as shown in Fig. S8 in the ESM, indicating that the process is irreversible and very likely to be the decomposition of electrolyte. Such irreversible decomposition could be the cause of the severe capacity fade in real batteries as shown in Fig. 4 and Fig. S9 in the ESM.

Herein, the effect of cut-off potential on electrolyte decomposition was also studied by *in situ* AFM. The pristine HOPG surfaces shown in Fig. 5(a) are clean and flat. Figure S10 in the ESM shows the AFM images taken at 4.19 to 4.72 V and 4.72 to 5.25 V during following charging process. No obvious electrolyte decomposition on the HOPG surface was found. Figure 5(b) shows the image obtained between 5.25 and 5.78 V. Figure 5(c) shows that there are three stages during the electrochemical process according to the change of surface profile along the dash line in Fig. 5(b). In Stage I at a low potential (below 4.8 V), the surface morphology barely changed. As the potential increased to 4.8 V, the average height started to increase owing to the intercalation of PF_6^- anion (Stage II). As the potential further increased to above 5.52 V, remarkable height increase was observed, which can be attributed to the uncontrollable electrolyte decomposition. The surface of HOPG was fully covered by thick layers (more than 50 nm) of decomposition products in Stage III. The components of the nanoparticles on the HOPG surface were analyzed by *ex situ* XPS. The spectra of C 1s and F 1s are shown in Fig. S11 in the ESM. Figures S11(a) and S11(b) in the ESM show the XPS results of HOPG before CV scanning. There are two obvious peaks in the C 1s spectra and they are located at 284.8 and 285 eV. They can be assigned to C–C bond and –C–O–C bond [7] respectively. After CV scanning, two new peaks arose at 287 and 289 eV as shown in Figs. S11(c) and S11(d) in the ESM. They can be assigned to –COOR and $-CO_3$. These products mainly came from the decomposition of solvents EC and DMC under the high potentials [7]. Figures S11(e) and S11(f)

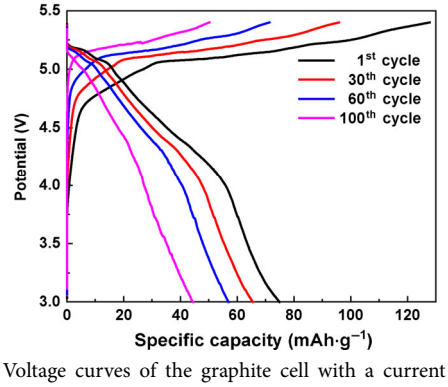

Figure 4 Voltage curves of the graphite cell with a current density of 20 mA·g^{-1} and voltage range of 3.0 to 5.5 V.

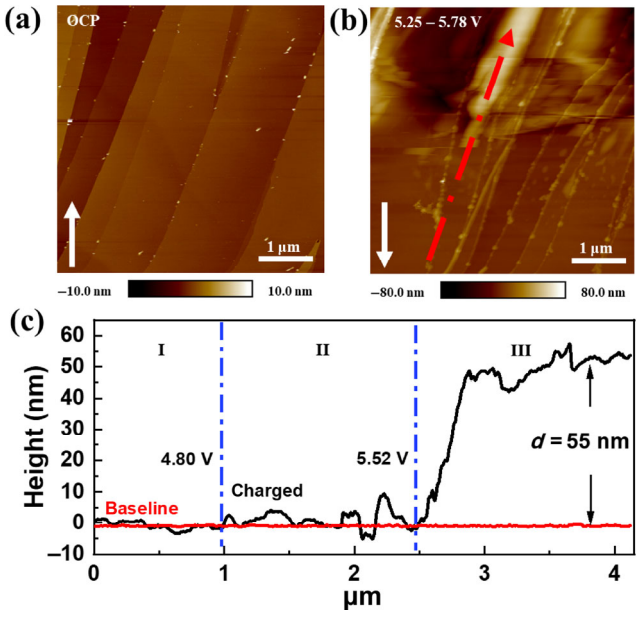

Figure 5 *In situ* AFM images with different cut-off potential. AFM images taken at (a) OCP, (b) 5.25 to 5.78 V. (c) The height profile along the dashed line in (b), the baseline in red was taken at OCP, and the black line represents the height after charge.

in the ESM show the spectra of F 1s, on the surface of HOPG, the two peaks which are located at 685 and 687 eV can be assigned to the LiF [7, 28] and $Li_xPF_yO_z$ [7, 28]. These fluorine containing products mainly come from the decomposition of PF_6^- under the high potentials [7]. It was previously reported that the graphite positive electrode in DIBs could also suffer from structural damage at high potentials during cycles [29]. Graphene layers would be oxidized to form blisters and even been exfoliated [23, 24, 30]. Figure 6 shows the graphite structure evolution during electrochemical process. Compared with the original HOPG surface (Fig. 6(a)), the flat HOPG surface appears to wrinkle (Fig. 6(b)) under a high potential. As exhibited in Fig. 6(d), the flat baseline became wavy after charging, which indicates the structural change of the graphite. The height of the selected step (black line) is shown in Fig. 6(e). The original height was 4 nm at OCP. The height change would be approximately 2 nm according to the intercalation mechanism as we demonstrated. However, in reality the height increased to 9 nm during sweeping voltage range of 5.07–5.60 V. After discharging, the height decreased to 7 nm. The reversible height change of 2 nm matches what we predicted using the proposed intercalation mechanism. Therefore, the irreversible height change of 3 nm can be attributed to the structural distortion of the graphite. The structural change is usually responsible for the capacity decay of an electrode material and should be prevented or minimized for better performance.

4 Conclusions

In summary, we successfully monitored the real-time interfacial and structure evolution of graphite in carbonate electrolyte utilizing *in situ* AFM. The anion (PF_6^-) intercalation mechanism and surface evolution can be summarized in Scheme 1. After anion intercalation which starts at 4.8 V, the interlayer spacing between two graphene layers was observed to increase by approximate 0.5 nm. Next, the anion intercalation behavior in multiple numbers of graphene layers was analyzed. Through many parallel *in situ* AFM experiments, the results show that anion intercalates in one of every three graphite layers. The time-dependent intercalation process observation at a fixed potential (4.8 V) was carried out and the PF_6^- anion intercalation speed was calculated as 2 μm·min^{-1}. Furthermore, by exploring the surface and structure evolution vs. rising potentials of the HOPG graphite, the stability of the carbonate electrolyte under high potentials was investigated. The electrolyte decomposition occurred firstly along the edges of HOPG, and then on the surface of HOPG. The decomposition continued in the following cycles. When a higher potential was applied, more severe decomposition was observed, along with structural distortion of the graphite. A high anion intercalation potential in DIBs not only affects the stability of the electrolyte but also the structure of the graphite positive electrode and would definitely decreases the stability and cycle performance in real cells.

These results will help researchers to get an in-depth understanding of the intercalation mechanism and surface reactions in DIBs and directions to improve battery performance.

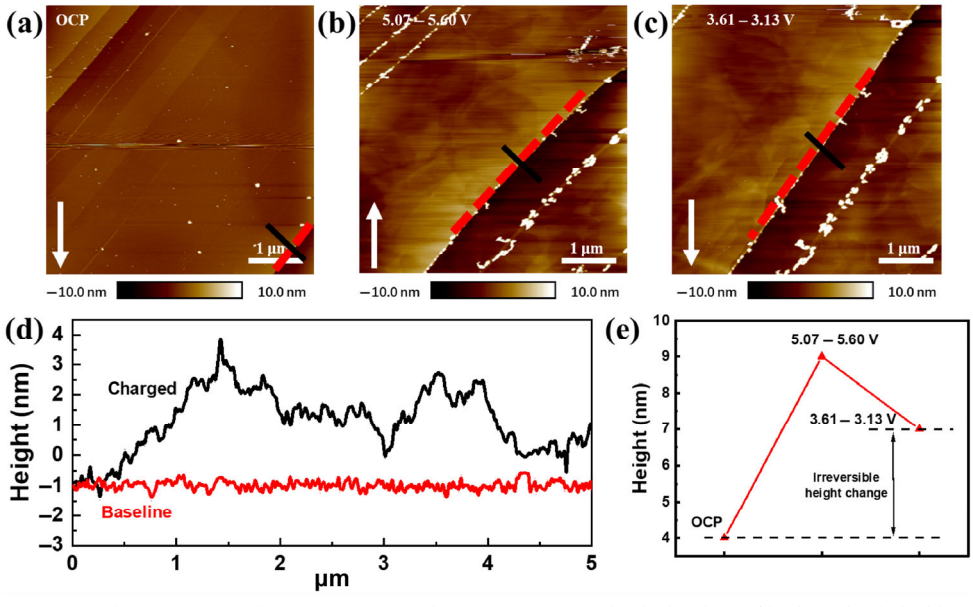

Figure 6 *In situ* AFM images taken at (a) OCP, (b) 5.07 to 5.60 V and (c) 3.61 to 3.13 V. (d) The height profile along the dashed line in AFM images, the baseline in red was taken at OCP, and the black line represents the height after charge. (e) The height changes of the selected step (black line in AFM images).

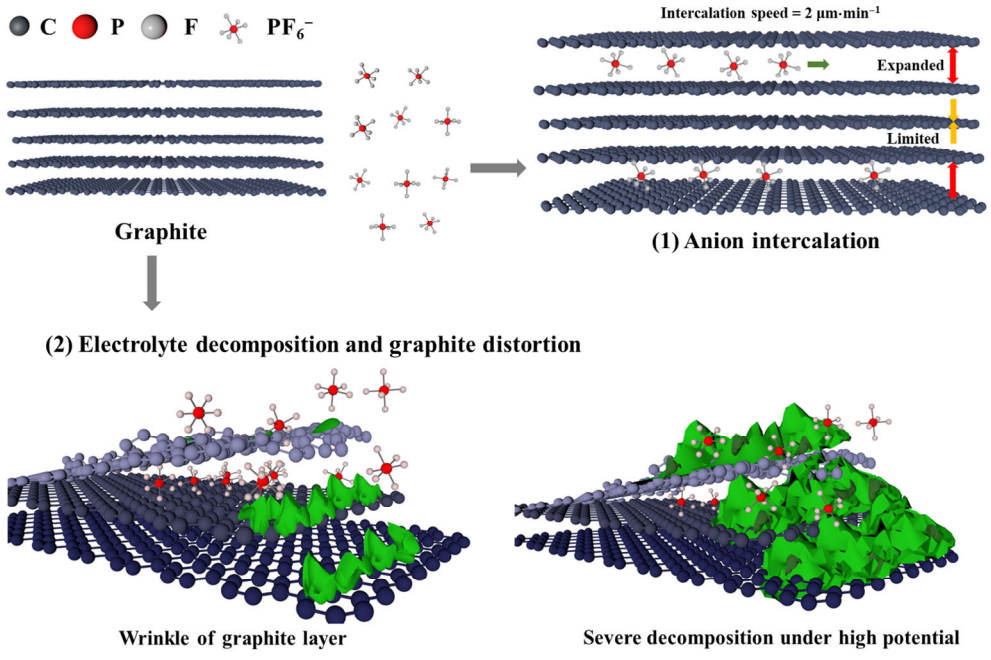

Scheme 1 A model showing the surface reaction and anion intercalation mechanism in graphite.

Acknowledgements

This research was financially supported by Soft Science Research Project of Guangdong Province (No. 2017B030301013) and the Shenzhen Science and Technology Research (Nos. JCYJ20170818085823773 and ZDSYS201707281026184).

Electronic Supplementary Material: Supplementary material (definition of parameters; additional electrochemical tests; additional AFM graphs; comparison and summary of previous works) is available in the online version of this article at https://doi.org/10.1007/s12274-020-2623-1.

References

[1] Wang, M.; Tang, Y. B. A review on the features and progress of dual-ion batteries. *Adv. Energy Mater.* **2018**, *8*, 1703320.

[2] Lu, J.; Chen, Z. W.; Pan, F.; Cui, Y.; Amine, K. High-performance anode materials for rechargeable lithium-ion batteries. *Electrochem. Energy Rev.* **2018**, *1*, 35–53.

[3] Zhou, Z. L.; Li, N.; Yang, Y. Z.; Chen, H. S.; Jiao, S. Q.; Song, W. L.; Fang, D. N. Ultra-lightweight 3D carbon current collectors: Constructing all-carbon electrodes for stable and high energy density dual-ion batteries. *Adv. Energy Mater.* **2018**, *8*, 1801439.

[4] Placke, T.; Heckmann, A.; Schmuch, R.; Meister, P.; Beltrop, K.; Winter, M. Perspective on performance, cost, and technical challenges for practical dual-ion batteries. *Joule* **2018**, *2*, 2528–2550.

[5] Gao, J. C.; Tian, S. F.; Qi, L.; Wang, H. Y. Intercalation manners of perchlorate anion into graphite electrode from organic solutions. *Electrochim. Acta* **2015**, *176*, 22–27.

[6] Kravchyk, K. V.; Bhauriyal, P.; Piveteau, L.; Guntlin, C. P.; Pathak, B.; Kovalenko, M. V. High-energy-density dual-ion battery for stationary storage of electricity using concentrated potassium fluorosulfonylimide. *Nat. Commun.* **2018**, *9*, 4469.

[7] Qi, X.; Blizanac, B.; DuPasquier, A.; Meister, P.; Placke, T.; Oljaca, M.; Li, J.; Winter, M. Investigation of PF_6^- and $TFSI^-$ anion intercalation into graphitized carbon blacks and its influence on high voltage lithium ion batteries. *Phys. Chem. Chem. Phys.* **2014**, *16*, 25306–25313.

[8] Wang, S.; Jiao, S. Q.; Tian, D. H.; Chen, H. S.; Jiao, H. D.; Tu, J. G.; Liu, Y. J.; Fang, D. N. A novel ultrafast rechargeable multi-ions battery. *Adv. Mater.* **2017**, *29*, 1606349.

[9] Jiao, S. Q.; Lei, H. P.; Tu, J. G.; Zhu, J.; Wang, J. X.; Mao, X. H. An industrialized prototype of the rechargeable Al/$AlCl_3$-[EMIm]Cl/graphite battery and recycling of the graphitic cathode into graphene. *Carbon* **2016**, *109*, 276–281.

[10] Sun, H. B.; Wang, W.; Yu, Z. J.; Yuan, Y.; Wang, S.; Jiao, S. Q. A new aluminium-ion battery with high voltage, high safety and low cost. *Chem. Commun.* **2015**, *51*, 11892–11895.

[11] Yu, Z. J.; Jiao, S. Q.; Li, S. J.; Chen, X. D.; Song, W. L.; Teng, T.; Tu, J. G.; Chen, H. S.; Zhang, G. H.; Fang, D. N. Flexible stable solid-state Al-ion batteries. *Adv. Funct. Mater.* **2019**, *29*, 1806799.

[12] Zhang, X. F.; Jiao, S. Q.; Tu, J. G.; Song, W. L.; Xiao, X.; Li, S. J.; Wang, M. Y.; Lei, H. P.; Tian, D. H.; Chen, H. S. et al. Rechargeable ultrahigh-capacity tellurium–aluminum batteries. *Energy Environ. Sci.* **2019**, *12*, 1918–1927.

[13] Placke, T.; Schmuelling, G.; Kloepsch, R.; Meister, P.; Fromm, O.; Hilbig, P.; Meyer, H. W.; Winter, M. *In situ* X-ray diffraction studies of cation and anion intercalation into graphitic carbons for electrochemical energy storage applications. *Z. Anorg. Allg. Chem.* **2014**, *640*, 1996–2006.

[14] Schmuelling, G.; Placke, T.; Kloepsch, R.; Fromm, O.; Meyer, H. W.; Passerini, S.; Winter, M. X-ray diffraction studies of the electrochemical intercalation of bis(trifluoromethanesulfonyl)imide anions into graphite for dual-ion cells. *J. Power Sources* **2013**, *239*, 563–571.

[15] Gao, J. C.; Yoshio, M.; Qi, L.; Wang, H. Y. Solvation effect on intercalation behaviour of tetrafluoroborate into graphite electrode. *J. Power Sources* **2015**, *278*, 452–457.

[16] Li, N.; Xin, Y. D.; Chen, H. S.; Jiao, S. Q.; Jiang, H. Q.; Song, W. L.; Fang, D. N. Thickness evolution of graphite-based cathodes in the dual ion batteries via *in operando* optical observation. *J. Energy Chem.* **2019**, *29*, 122–128.

[17] Cresce, A. V.; Russell, S. M.; Baker, D. R.; Gaskell, K. J.; Xu, K. *In situ* and quantitative characterization of solid electrolyte interphases. *Nano Lett.* **2014**, *14*, 1405–1412.

[18] Liu, T. C.; Lin, L. P.; Bi, X. X.; Tian, L. L.; Yang, K.; Liu, J. J.; Li, M. F.; Chen, Z. H.; Lu, J.; Amine, K. et al. *In situ* quantification of interphasial chemistry in Li-ion battery. *Nat. Nanotechnol.* **2019**, *14*, 50–56.

[19] Lacey, S. D.; Wan, J. Y.; von Wald Cresce, A.; Russell, S. M.; Dai, J. Q.; Bao, W. Z.; Xu, K.; Hu, L. B. Atomic force microscopy studies on molybdenum disulfide flakes as sodium-ion anodes. *Nano Lett.* **2015**, *15*, 1018–1024.

[20] Liu, C.; Ye, S. *In situ* Atomic Force Microscopy (AFM) study of oxygen reduction reaction on a gold electrode surface in a dimethyl sulfoxide (DMSO)-based electrolyte solution. *J. Phys. Chem. C* **2016**, *120*, 25246–25255.

[21] Liu, X. R.; Wang, L.; Wan, L. J.; Wang, D. *In situ* observation of electrolyte-concentration-dependent solid electrolyte interphase on graphite in dimethyl sulfoxide. *ACS Appl*. *Mater*. *Interfaces* **2015**, *7*, 9573–9580.

[22] Alliata, D.; Häring, P.; Haas, O.; Kötz, R.; Siegenthaler, H. Anion intercalation into highly oriented pyrolytic graphite studied by electrochemical atomic force microscopy. *Electrochem*. *Commun*. **1999**, *1*, 5–9.

[23] Alliata, D.; Kötz, R.; Haas, O.; Siegenthaler, H. *In situ* AFM study of interlayer spacing during anion intercalation into HOPG in aqueous electrolyte. *Langmuir* **1999**, *15*, 8483–8489.

[24] Goss, C. A.; Brumfield, J. C.; Irene, E. A.; Murray, R. W. Imaging the incipient electrochemical oxidation of highly oriented pyrolytic graphite. *Anal*. *Chem*. **1993**, *65*, 1378–1389.

[25] Noel, M.; Santhanam, R. Electrochemistry of graphite intercalation compounds. *J*. *Power Sources* **1998**, *72*, 53–65.

[26] Ishihara, T.; Yokoyama, Y.; Kozono, F.; Hayashi, H. Intercalation of PF_6^- anion into graphitic carbon with nano pore for dual carbon cell with high capacity. *J*. *Power Sources* **2011**, *196*, 6956–6959.

[27] Seel, J. A.; Dahn, J. R. Electrochemical intercalation of PF_6^- into graphite. *J*. *Electrochem*. *Soc*. **2000**, *147*, 892–898.

[28] Eshetu, G. G.; Diemant, T.; Grugeon, S.; Behm, R. J.; Laruelle, S.; Armand, M.; Passerini, S. In-depth interfacial chemistry and reactivity focused investigation of lithium–imide-and lithium–imidazole-based electrolytes. *ACS Appl*. *Mater*. *Interfaces* **2016**, *8*, 16087–16100.

[29] Märkle, W.; Tran, N.; Goers, D.; Spahr, M. E.; Novák, P. The influence of electrolyte and graphite type on the PF_6^- intercalation behaviour at high potentials. *Carbon* **2009**, *47*, 2727–2732.

[30] Choo, H. S.; Kinumoto, T.; Jeong, S. K.; Iriyama, Y.; Abe, T.; Ogumi, Z. Mechanism for electrochemical oxidation of highly oriented pyrolytic graphite in sulfuric acid solution. *J*. *Electrochem*. *Soc*. **2007**, *154*, B1017–B1023.